Computation of the flow and heat transfer due to a rotating disc

C. L. Ong* and J. M. Owen†
Thermo-Fluid Mechanics Research Centre, University of Sussex, Falmer, Brighton, UK

The boundary-layer momentum and energy equations have been solved numerically using a Keller-box scheme and, for turbulent flow, an eddy-viscosity model. The numerical method has been successfully validated on a number of standard test cases for unheated discs, including data for velocity profiles and moment coefficients in both laminar and turbulent flow, and some old and new test cases for heated discs, including average and local Nusselt numbers for a range of disc-temperature distributions and for Reynolds numbers up to 3.2×10^6. The method is shown to be sufficiently simple, efficient, and accurate for all practical purposes.

Keywords: rotating disc; heat transfer; free disc; rotating flow

1. Introduction

A simple rotating disc can be used to model the more complicated flows that occur inside the rotors of turbomachinery. In most practical applications, the disc usually rotates close to a stationary casing or corotates with other discs, as is the case for turbine and compressor discs in a gas-turbine engine. However, in order to understand these flows, it is helpful to study first the case of a single disc rotating in an infinite quiescent environment: the so-called free disc.

Laminar flow over the free disc, which was first studied by von Kármán[1] and solved numerically by Cochran,[2] provides one of the few cases for which exact solutions of the Navier–Stokes equations exist. For a disc rotating with an angular speed Ω in a fluid with kinematic viscosity ν, a boundary layer with a uniform thickness of order $(\nu/\Omega)^{1/2}$ forms on either side of the disc. Inside the boundary layer, the tangential component of velocity, v_ϕ, is sheared from Ωr at the surface of the disc to zero in the "free stream." "Centrifugal forces" cause a radial outflow of fluid inside the boundary layer, and fresh fluid is entrained axially, as shown in Figure 1. In practice, the flow inside the boundary layer can be laminar or turbulent, and for a smooth disc the most important determining parameter is the local Reynolds number, $\Omega r^2/\nu$, where r is the radial location. For large values of Ω, the flow may be laminar near the center of the disc and turbulent at large radii, with a transition zone between the laminar and turbulent boundary layers.

The free-disc fluid-dynamics problems have been studied theoretically using analytical techniques for laminar flow and using integral and numerical methods for turbulent flow. Further details of these are given by Owen and Rogers,[3] but the papers of most relevance to the numerical method described below are those of Cooper,[4] Koosinlin,[5] and Launder and Sharma,[6] and Cebeci and Abbott.[7] Cooper and Cebeci and Abbott modeled the Reynolds-stress terms by an isotropic eddy-viscosity turbulence model proposed by Cebeci and Smith.[8] Koosinlin assessed both isotropic and anisotropic mixing-length models, and Launder and Sharma used the low-Reynolds-number version of the k–ε turbulence model developed by Jones and Launder.[9]

In the present work the fluid-dynamics problems of the free disc are revisited, using a method similar to that employed by Cebeci and Abbott, and a fresh look is taken at the heat-transfer case. The boundary-layer equations and turbulence model are discussed in Section 2, and the numerical method of solution is described in Section 3. Section 4 includes comparisons between the computed results and experimental data for velocity profiles and moment coefficients, and Section 5 contains comparisons between computed and measured average and local Nusselt numbers.

2. Boundary-layer equations and turbulence model

2.1 Boundary-layer equations

For the steady, incompressible, axisymmetric boundary layer formed on the rotating disc, in the absence of a radial pressure

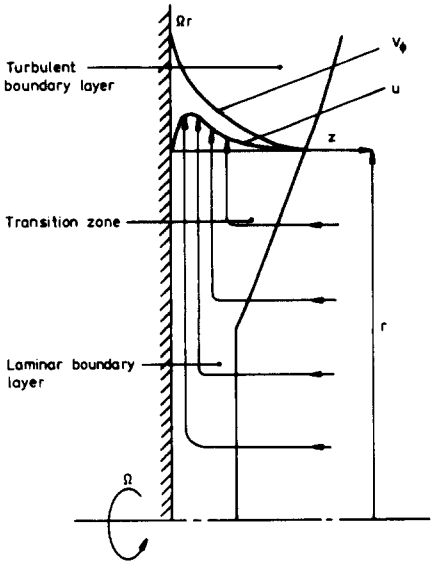

Figure 1 Simplified diagram of flow over the free disc

Address reprint requests to Prof. Owen at the School of Mechanical Engineering, University of Bath, Claverton Down, Bath, BA2 7AY, UK.

Received 26 April 1990; accepted 16 July 1990

* Now at National Grid Company plc, Research and Development Centre, Leatherhead, Surrey, UK
† Now at School of Mechanical Engineering, University of Bath, Bath, UK

gradient, the governing continuity, momentum, and energy equations may be expressed in a stationary cylindrical coordinate (r, ϕ, z) system (see Owen and Rogers[3]) as

- continuity

$$\frac{1}{r}\frac{\partial}{\partial r}(ru)+\frac{\partial w}{\partial z}=0 \tag{2.1}$$

- r momentum

$$u\frac{\partial u}{\partial r}+w\frac{\partial u}{\partial z}-\frac{v_\phi^2}{r}=-\frac{1}{\rho}\frac{\partial \tau_r}{\partial z} \tag{2.2}$$

- ϕ momentum

$$u\frac{\partial v_\phi}{\partial r}+w\frac{\partial v_\phi}{\partial z}+\frac{uv_\phi}{r}=-\frac{1}{\rho}\frac{\partial \tau_\phi}{\partial z} \tag{2.3}$$

- energy

$$u\frac{\partial h}{\partial r}+w\frac{\partial h}{\partial z}=-\frac{1}{\rho}\frac{\partial}{\partial z}(-q+u\tau_r+v_\phi\tau_\phi) \tag{2.4}$$

where the total enthalpy, h, is given by

$$h=C_pT+\tfrac{1}{2}(u^2+v_\phi^2) \tag{2.5}$$

For turbulent flow, employing the concepts of effective exchange coefficients, the radial and tangential shear-stress components, τ_r and τ_ϕ, and the heat flux, q, are defined by

$$\frac{1}{\rho}\tau_r=\nu_{\text{eff}}\frac{\partial u}{\partial z} \qquad \frac{1}{\rho}\tau_\phi=\nu_{\text{eff}}\frac{\partial v_\phi}{\partial z} \tag{2.6}$$

and

$$q=-\rho C_p\left(\frac{\nu}{\text{Pr}_{\text{eff}}}\right)\frac{\partial T}{\partial z} \tag{2.7}$$

The effective viscosity, ν_{eff}, is the sum of the laminar and turbulent contributions, such that

$$\nu_{\text{eff}}=\nu+\nu_t \tag{2.8}$$

and the effective Prandtl number, Pr_{eff}, is related to the laminar and turbulent values by

$$\left(\frac{\nu}{\text{Pr}}\right)_{\text{eff}}=\frac{\nu}{\text{Pr}}+\frac{\nu_t}{\text{Pr}_t} \tag{2.9}$$

For the results presented in this article, the turbulent Prandtl number, Pr_t, is taken to be constant with a value of 0.9. For laminar flow, the eddy viscosity, ν_t, is zero; for turbulent flow, the formulation is given in Section 2.2.

Boundary conditions for the velocity field are given by the

Notation

A^+	Van Driest's damping constant
b	Outer radius of disc
C_m	Moment coefficient, $2M/\frac{1}{2}\rho\Omega^2b^5$
C_p	Specific heat at constant pressure
f	Nondimensional stream function, $\psi/r^2(\nu\Omega)^{1/2}$
f'	Nondimensional radial component of velocity, $u/\Omega r$
g	Nondimensional tangential component of velocity, $v_\phi/\Omega r$
G	Empirical factor, Equation 2.20
h	Total enthalpy
k	Thermal conductivity
l	Mixing length
M	Frictional moment on one side of the disc
n	Exponent in power law for temperature profiles
Nu	Local Nusselt number, $q_sr/k(T_s-T_\infty)$
Nu*	Local Nusselt number based on adiabatic-disc temperature, $q_sr/k(T_s-T_{s,\text{ad}})$
Pr	Prandtl number, $\mu C_p/k$
q	Heat flux
r	Radial coordinate
R	Recovery factor
Re_ϕ	Rotational Reynolds number, $\Omega b^2/\nu$
R_{δ_2}	Reynolds number based on swirl momentum thickness, $\delta_2\Omega r/\nu$
S	Derivative of nondimensional enthalpy, θ'
T	Temperature
u	Radial component of velocity
U	Derivative of nondimensional stream function, f'
v_ϕ	Tangential component of velocity
V	Second derivative of nondimensional stream function, $f''=U'$
w	Axial component of velocity
W	Derivative of nondimensional tangential velocity, g'
x	Nondimensional radius, r/b
z	Axial distance
z^+	Nondimensional axial distance, $z\tau_s^{1/2}/\nu\rho^{1/2}$
z_c	Axial location at which $\nu_{t,i}=\nu_{t,o}$

Greek symbols

α	Outer eddy-viscosity coefficient
β	Nondimensional effective viscosity
γ_{tr}	Transition intermittency factor
δ	Boundary-layer thickness
δ_2	Swirl momentum thickness
$\varepsilon_1, \varepsilon_2$	Error tolerances
η	Transformed z coordinate, $(\Omega/\nu)^{1/2}z$
θ	Nondimensional enthalpy profile
κ	Von Karman's mixing-length constant
μ	Dynamic viscosity
ν	Kinematic viscosity, μ/ρ
ρ	Density
ξ	Function in relationship between h and θ
τ	Resultant shear stress, $(\tau_r^2+\tau_\phi^2)^{1/2}$
τ_r	Radial component of shear stress
τ_ϕ	Tangential component of shear stress
τ^+	Nondimensional local shear stress, τ/τ_s
ϕ	Angular coordinate
χ	Cole's profile parameter, Equation 2.18
ψ	Stream function
Ω	Angular speed of the disc

Subscripts

ad	Adiabatic-disc condition
av	Radially weighted average
eff	Effective value
i	Inner region of boundary layer
o	Outer region of boundary layer
ref	Reference value
s	Value at the disc surface
t	Turbulent value
tr	Transitional value
∞	Ambient value

no-slip and no-penetration conditions on the disc as follows:

$$\begin{aligned} &z=0: \quad u=w=0 \qquad v_\phi=\Omega r \\ &z\to\infty: \quad u, v_\phi \to 0 \end{aligned} \tag{2.10}$$

For the energy equation,

$$\begin{aligned} z=0 \text{ and disc temperature specified:} \quad & T=T_s \\ z=0 \text{ and disc flux specified:} \quad & q=q_s \\ z\to\infty: \quad & T\to T_\infty \end{aligned} \tag{2.11}$$

where T_∞ is the ambient temperature.

To complete the formulation of the problem, initial conditions must be specified at the starting radius for the velocity and temperature distributions. Here, the radial velocity is assumed to be zero, and the tangential velocity and the temperature are assumed to decrease linearly with the distance z from the disc surface, such that

$$\begin{aligned} &u=0 \\ &v_\phi=\left(1-\frac{z}{z_\infty}\right)\Omega r \qquad 0\leqslant z\leqslant z_\infty \\ &T=T_s+(T_\infty-T_s)\left(\frac{z}{z_\infty}\right) \end{aligned} \tag{2.12}$$

where z_∞ is a chosen value greater than the theoretical laminar boundary-layer thickness δ. For convenience, it was assumed that $\delta=3.6(\nu/\Omega)^{1/2}$, which corresponds to the axial location where Cochran's solutions[2] show that $v_\phi/\Omega r=0.05$; in practice, a value of z_∞ equal to $8(\nu/\Omega)^{1/2}$ has been found to be satisfactory.

2.2 Turbulence model

The turbulence model employed here is an adaptation of the isotropic eddy-viscosity formulation proposed by Cebeci and Smith,[8] which can account for various observed free-disc boundary-layer effects. According to this formulation, the boundary layer is assumed to comprise inner and outer axial regions, denoted here by the subscripts i and o, respectively.

For the inner region, close to the disc surface, ν_t is based on Prandtl's mixing-length hypothesis. Using the resultant mean-velocity gradient for the swirling boundary layer on the disc, $\nu_{t,i}$ is given by

$$\nu_{t,i}=l^2\left[\left(\frac{\partial u}{\partial z}\right)^2+\left(\frac{\partial v_\phi}{\partial z}\right)^2\right]^{1/2} \qquad 0<z\leqslant z_c \tag{2.13}$$

where z_c is the axial location at which $\nu_{t,i}=\nu_{t,o}$. The mixing length, l, is defined by

$$l=\kappa z\{1-\exp[-z^+(\tau^+)/A^+]\} \tag{2.14}$$

where z^+ and τ^+ are, respectively, the nondimensional axial distance and local shear stress given by

$$z^+=\frac{z\tau_s^{1/2}}{\nu\rho^{1/2}} \quad \text{and} \quad \tau^+=\frac{\tau}{\tau_s} \tag{2.15}$$

with τ_s being the resultant wall shear stress. By convention, the empirical constants κ and A^+ are assigned the values of 0.4 and 26.0, respectively.

For the outer region of the boundary layer,

$$\nu_{t,o}=\alpha\left|\int_0^\infty \{\Omega r-[u^2+(\Omega r-v_\phi)^2]\}\,dz\right| \qquad z_c\leqslant z \tag{2.16}$$

Continuity between the inner and outer regions is maintained by choosing $\nu_t=\min(\nu_{t,i}, \nu_{t,o})$. The parameter α in Equation 2.16 is usually assumed to be a universal constant equal to 0.0168 for flow at high Reynolds number. However, according to Cebeci,[10] at low Reynolds numbers, α is a function of the Reynolds number, such that

$$\alpha=0.0168\left(\frac{1.55}{1+\chi}\right) \tag{2.17}$$

where χ is given by the empirical expression

$$\chi=0.55[1-\exp(-0.243y^{1/2}-0.298y)] \tag{2.18}$$

with $y=R_{\delta_2}/425-1$ for $R_{\delta_2}>425$ and $y=0$ for $R_{\delta_2}\leqslant 425$. For a swirling boundary layer, R_{δ_2} is the Reynolds number based on the swirl momentum thickness δ_2 such that $R_{\delta_2}=\delta_2\Omega r/\nu$ and

$$\delta_2=\int_0^\infty \left|\frac{v_\phi}{\Omega r}\left(1-\frac{v_\phi}{\Omega r}\right)\right| dz \tag{2.19}$$

The eddy-viscosity formulation given by Equations 2.13 and 2.16 is based on empirical correlations obtained for fully turbulent flows and therefore should not be expected to give a good representation of the transition from laminar to turbulent flow. According to experimental evidence (see Gregory et al.[11]), laminar flow becomes unstable on a smooth disc at $x^2Re_\phi\approx 1.8\times10^5$, and transition to turbulent flow is complete by $x^2Re_\phi\approx 3\times10^5$, where $x=r/b$, $Re_\phi=\Omega b^2/\nu$, and b is the radius of the disc. Following Cebeci and Abbott,[7] we accounted for the effects of transition by multiplying $\nu_{t,i}$ and $\nu_{t,o}$ by an intermittency factor, γ_{tr}, given by

$$\begin{aligned} &\gamma_{tr}=1-\exp[-G(1-x_{tr}/x)^2] \\ &G=8.35\times10^{-4}(x^2Re_\phi)^2(x_{tr}^2Re_\phi)^{-1.34} \end{aligned} \tag{2.20}$$

where x_{tr} is the nondimensional radial location of the start of transition.

3. Numerical method

3.1 Transformation of the momentum equations

Although Equations 2.1–2.3 may be solved directly, it is more convenient to transform them by using a similarity variable, η, where

$$\eta=\left(\frac{\Omega}{\nu}\right)^{1/2}z \tag{3.1}$$

and by introducing a nondimensional stream function $f(r,\eta)$ defined as

$$f=\frac{\psi(r,z)}{r^2(\nu\Omega)^{1/2}} \tag{3.2}$$

Here, $\psi(r,z)$ is the stream function for which

$$ur=\frac{\partial\psi}{\partial z} \quad \text{and} \quad wr=-\frac{\partial\psi}{\partial r} \tag{3.3}$$

such that continuity Equation 2.1 is satisfied.

With the introduction of an additional nondimensional variable $g(r,\eta)$ given by

$$g=\frac{v_\phi}{\Omega r} \tag{3.4}$$

Equations 2.2 and 2.3 can be expressed as

$$(\beta f'')'+2ff''-(f')^2+g^2=r\left(f'\frac{\partial f'}{\partial r}-f''\frac{\partial f}{\partial r}\right) \tag{3.5}$$

$$(\beta g')'+2fg'-2f'g'=r\left(f'\frac{\partial g}{\partial r}-g'\frac{\partial f}{\partial r}\right) \tag{3.6}$$

where

$$\beta=1+\nu_t^+, \qquad \nu_t^+=\frac{\nu_t}{\nu} \tag{3.7}$$

and the primes denote differentiation with respect to η.

In terms of the transformed variables, the appropriate boundary conditions, corresponding to Equations 2.10, become:

$$\begin{aligned}&\eta=0: \quad f=f'=0 \quad g=1\\ &\eta\to\infty: \quad f'=g=0\end{aligned} \tag{3.8}$$

Use of the similarity variable, η, results in a transformed boundary layer of constant thickness for laminar flow [where $\delta\propto(\nu/\Omega)^{1/2}$], and it also provides a convenient scaling factor for turbulent flow. (Initial conditions for f and g are provided by Equation 2.12).

3.2 Transformation of the energy equation

As for the momentum equations, it is useful to express the governing energy Equation 2.4 in terms of nondimensional transformed variables before it is solved. This is achieved by introducing a further nondimensional variable, $\theta(r,\eta)$, such that

$$h(r,\eta)=h_\infty(r)[1+\theta(r,\eta)\xi(r)] \tag{3.9}$$

where $\xi(r)$ is a function that is specified according to the thermal boundary conditions used.

For specified disc temperature, T_s (implying known enthalpy), ξ is chosen to be

$$\xi=\frac{h_s-h_\infty}{h_\infty} \tag{3.10}$$

giving the definition

$$\theta=\frac{h-h_\infty}{h_s-h_\infty} \tag{3.11}$$

such that, like g, θ is unity at the disc surface and zero at infinity.

If the heat flux, $q_s=-k(\partial T/\partial z)_{z=0}$, is specified, it follows from Equations 2.5 and 3.9 that

$$q_s=-\frac{kh_\infty}{C_p}\left(\frac{\Omega}{\nu}\right)^{1/2}\left[\xi(r)\theta'(r,0)-\frac{\Omega^2r^2}{h_\infty}g'(r,0)\right] \tag{3.12}$$

For this case, it is convenient to define ξ as

$$\xi=-\frac{q_sC_p}{kh_\infty}\left(\frac{\nu}{\Omega}\right)^{1/2}+\frac{\Omega^2r^2g'(r,0)}{h_\infty} \tag{3.13}$$

such that θ' is unity at the disc surface.

Utilizing Equation 3.9 together with Equations 3.1–3.4, we can write the energy Equation 2.4 in nondimensional transformed variables as

$$(\zeta\theta')'-\sigma f'\theta+2f'\theta'=r\left(f'\frac{\partial\theta}{\partial r}-\theta'\frac{\partial f'}{\partial r}\right)-[\gamma(f'f''+gg')]' \tag{3.14}$$

where

$$\begin{aligned}\zeta&=\frac{1}{\mathrm{Pr}}\left(1+\frac{\mathrm{Pr}}{\mathrm{Pr}_t}\nu_t^+\right)\\ \gamma&=\frac{\Omega^2r^2}{h_\infty\xi}\left[1-\frac{1}{\mathrm{Pr}}+\nu_t^+\left(1-\frac{1}{\mathrm{Pr}_t}\right)\right]\end{aligned} \tag{3.15}$$

and σ is a nondimensional parameter defined for the case of given disc temperature by

$$\sigma=\frac{r}{T_s-T_\infty}\frac{d}{dr}(T_s-T_\infty) \tag{3.16}$$

and for given disc flux by

$$\sigma=\frac{r}{\xi}\frac{d\xi}{dr} \tag{3.17}$$

In terms of θ, the boundary conditions given by Equation 2.11 become

$$\begin{aligned}&\eta=0 \qquad a_1\theta_s+a_2\theta_s'=1\\ &\eta\to\infty \qquad \theta_\infty\to0\end{aligned} \tag{3.18}$$

For specified temperatures, $a_1=1$ and $a_2=0$; for specified flux, $a_1=0$ and $a_2=1$.

3.3 Solution procedure

The transformed momentum and energy Equations 3.5, 3.6, and 3.13 were converted, through the introduction of auxiliary variables $U(r,\eta)$, $V(r,\eta)$, $W(r,\eta)$, and $S(r,\eta)$ to a system of seven first-order differential equations, as follows:

$$f'=U \tag{3.19}$$

$$U'=V \tag{3.20}$$

$$g'=W \tag{3.21}$$

$$(\beta V)'+2fV-U^2+g^2=r\left(U\frac{\partial U}{\partial r}-V\frac{\partial f}{\partial r}\right) \tag{3.22}$$

$$(\beta W)'+2fW-2Ug=r\left(U\frac{\partial g}{\partial r}-W\frac{\partial f}{\partial r}\right) \tag{3.23}$$

$$\theta'=S \tag{3.24}$$

$$(\zeta S)'-\sigma U\theta+2US=r\left(U\frac{\partial\theta}{\partial r}-S\frac{\partial U}{\partial r}\right)-[\gamma(UV+gW)]' \tag{3.25}$$

In terms of the new variables, the appropriate boundary conditions become

$$\begin{aligned}&\eta=0: \quad f(r,0)=U(r,0)=0 \qquad g(r,0)=1\\ &\qquad\quad a_1\theta(r,0)+a_2S(r,0)=1\\ &\eta\to\infty: \quad U(r,\infty)=W(r,\infty)=\theta(r,\infty)=0\end{aligned} \tag{3.26}$$

The complete system, Equations 3.19–3.25, was then discretized by use of the semi-implicit Keller-box[12] scheme. For incompressible flow, where the velocity field is independent of the temperature field, the sets of momentum and energy equations are uncoupled. At each radius, the nonlinear algebraic momentum equations were first solved following linearization by Newton's method, and the linear energy equations were then solved directly. Solutions of the 5×5 and 2×2 block systems for the momentum and energy equations, respectively, were accomplished by an efficient block-tridiagonal factorization technique.

The computations were started at radius $r=0$ where Equations 3.19–3.25 constitute a system of ordinary differential equations, since (for the similarity solutions that occur for laminar flow) the right-hand sides of Equations 3.22, 3.23, and 3.25 are identically zero.

The resulting local-similarity solutions should correspond to the exact laminar solutions first obtained by Cochran[2] for the full Navier–Stokes equations. In the present solution of this system of ordinary differential equations, at $r=0$, initial estimates for the dependent variables were given by Equation 2.12,

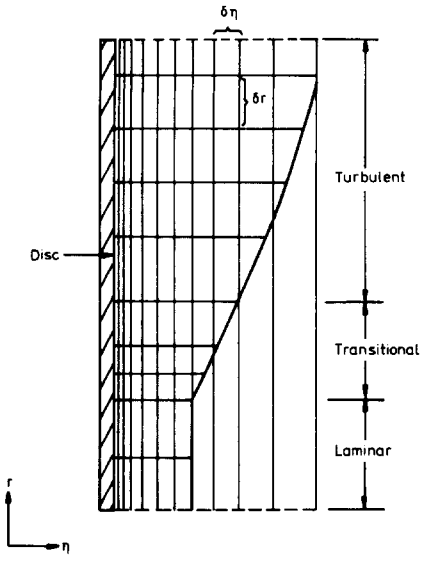

Figure 2 Finite-difference mesh used in the computation

which in terms of the new variables become:

$$f(0,\eta)=U(0,\eta)=V(0,\eta)=0$$

$$g(0,\eta)=\theta(0,\eta)=1-\frac{\eta}{\eta_\infty} \qquad 0\leqslant\eta\leqslant\eta_\infty \tag{3.27}$$

$$W(0,\eta)=S(0,\eta)=-\frac{1}{\eta_\infty}$$

A marching procedure was adopted, which advanced radially outwards on a grid having a variable spacing in the radial direction and a geometrically increasing spacing in the axial direction, as illustrated in Figure 2. For turbulent flow, the grids were concentrated near the disc surface, where gradients are larger; this allowed good resolution in the viscous sublayer and a coarse mesh toward the edge of the boundary layer. However, for laminar flow, where gradients are less severe and the boundary layer is of constant thickness, it was found satisfactory to use a uniform mesh in the axial direction, typically of 100 nodes with a nondimensional spacing of $\eta=0.08$.

For the turbulent-flow computations presented, a geometric progression was used with the first nondimensional axial grid spacing of 0.01 and an expansion factor of 1.05. This grid distribution produces a number of axial nodes that typically increased from about 80 at $r=0$ to 140 at a radius corresponding to $x^2\mathrm{Re}_\phi=10^7$. This increase in grids corresponds, approximately, to the increase in computed boundary-layer thickness with radius, and there were always at least 10 nodes in the viscous sublayer.

Two different criteria were adopted to ensure that the axial domain of computation was sufficiently large to encompass the important flow and temperature details. At each radial location, one of the following checks was made after convergence of the solution: either

$$|W(r,\infty)|, \qquad |S(r,\infty)|\leqslant\varepsilon_1$$

or

$$\{[V(r,\infty)]^2+[W(r,\infty)]^2\}^{1/2}\leqslant\varepsilon_2 \quad \text{and} \quad |S(r,\infty)|\leqslant\varepsilon_1$$

where the tolerances ε_1 and ε_2 were typically 0.001 and 0.01, respectively. Either check has been found to be effective in determining the extent of the momentum and thermal boundary layers beyond which the velocity components and temperature may be taken to equal their values at infinity. If the condition programmed was not satisfied, further points were added to the domain of computation and the procedure repeated.

By the above process, the axial calculation domain, $\eta_{\infty,j}$, at the radial location r_j became greater than that at the previous radial location r_{j-1}. Since, at r_j, the upstream values of the dependent variables and their derivatives were obtained from values at r_{j-1}, it was necessary to extrapolate their values for $\eta>\eta_{\infty,j-1}$. Hence in this region, f was given by

$$f(r_{j-1},\eta)=[\eta-\eta_{\infty,j-1}]U(r_{j-1,\infty})+f(r_{j-1,\infty})$$

with $U(r_j,\eta)$ taken to be $U(r_j,\eta_\infty)$ and $V(r_j,\eta)$ to be zero. Values for $g(r_j,\eta)$ and $\theta(r_j,\eta)$ were taken to be their values at (r_j,η_∞) and their derivatives were consequently zero.

Further details of the numerical method are given by Ong,[13] and typical run times were approximately 5 min on a VAX 8530 computer.

4. Results for an unheated disc

The finite-difference procedure described was used, with a grid of 50 radial nodes, to compute the flow in the boundary layer from zero radius to that corresponding to $x^2\mathrm{Re}_\phi=10^7$. The computations were compared to theoretical results for laminar flow and to experimental data for laminar, transitional, and turbulent flow. (Most of the experimental data were extracted manually from graphs in the publications cited.)

4.1 Velocity profiles

The difference between the computed velocity profile for laminar flow and Cochran's results[2] was less than 0.5%. The nondimensional shear stress, $g'(r,0)$, was computed to be -0.616, which agrees exactly with Cochran's value (which was given to an accuracy of three significant places).

Figure 3 shows the comparison between the computed tangential component of velocity and the measured values of Theodorsen and Regier.[14] In Figure 3a ($x^2\mathrm{Re}_\phi=2.72\times10^5$), the flow was assumed to be laminar; for the other results, transition was assumed to start at $x_{\mathrm{tr}}^2\mathrm{Re}_\phi=3\times10^5$. Agreement between the computed and measured velocities is good, particularly at the higher Reynolds numbers.

Figures 4 and 5 show the comparison between the computed tangential and radial components of velocity and the measured values of Cham and Head;[15] the abscissa, δ_2, is the momentum thickness defined by Equation 2.19. It can be seen that the computed tangential components of velocity provide a good fit to the experimental data, whereas the computed radial components tend to underestimate both the maximum value and the value at the outer edge of the boundary layer.

4.2 Moment coefficients

The moment coefficient, C_m, is defined as

$$C_m=\frac{2M}{\frac{1}{2}\rho\Omega^2b^5} \tag{4.1}$$

where

$$M=-2\pi\int_0^b r^2\tau_{\phi,\mathrm{s}}\,dr \tag{4.2}$$

and

$$\tau_{\phi,\mathrm{s}}=-\mu\left(\frac{\partial v_\phi}{\partial z}\right)_{z=0} \tag{4.3}$$

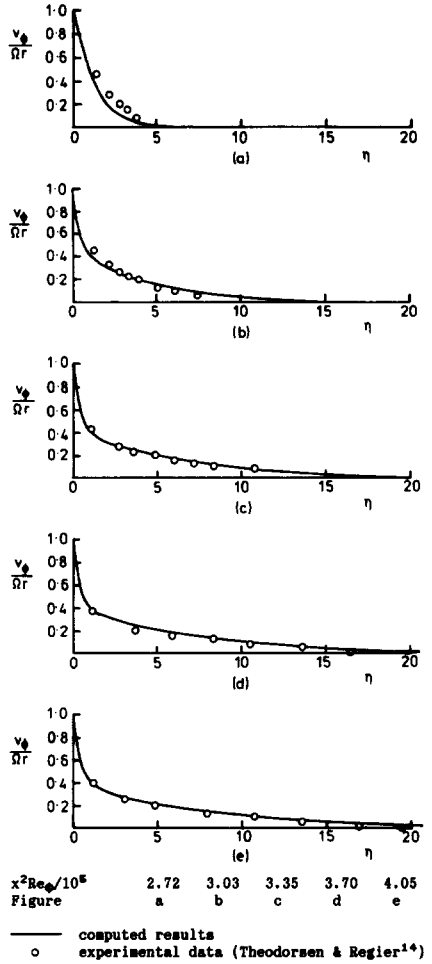

Figure 3 Axial profiles of tangential component of velocity for laminar and transitional flow over the free disc

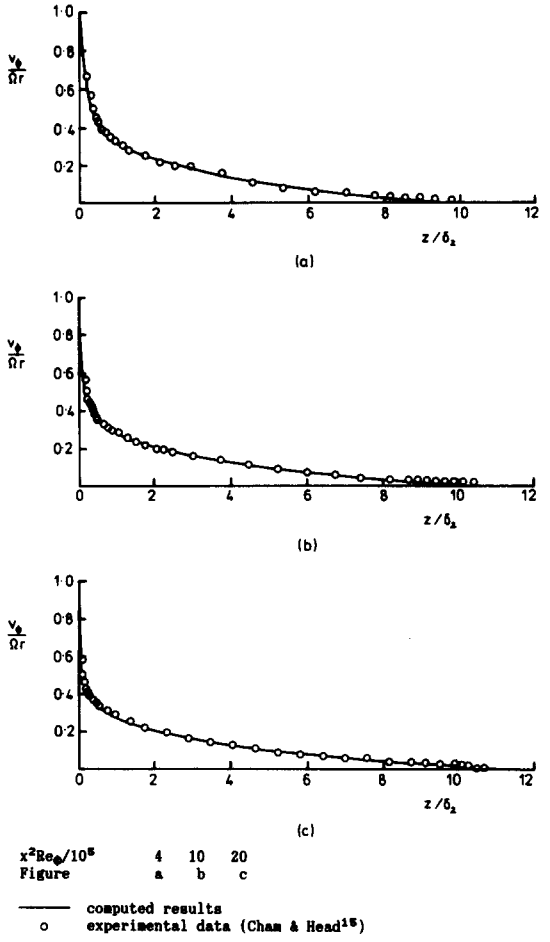

Figure 4 Axial profiles of tangential component of velocity for turbulent flow over the free disc

In terms of the transformed variables,

$$C_m=\frac{8\pi}{b^5}\left(\frac{\nu}{\Omega}\right)^{1/2}\int_0^b r^3 g'(r,0)\,dr \tag{4.4}$$

For laminar flow, where $g'(r,0)=0.6159$,

$$C_m=3.87\mathrm{Re}_\phi^{-1/2} \tag{4.5}$$

which agrees exactly with Cochran's solution.

Computations were carried out for turbulent flow for three different cases.

(i) Transition begins and ends at $x^2\mathrm{Re}_\phi=3\times10^5$.
(ii) Transition is modeled by the introduction of an intermittency factor, γ_{tr} (see Equation 2.19), with $x_{tr}^2\mathrm{Re}_\phi=1.85\times10^5$.
(iii) Turbulent flow occurs for all $x^2\mathrm{Re}_\phi$.

A comparison between the computed moment coefficients and the measurements of Theodorsen and Regier[14] and Owen[16] are shown in Figure 6. Both cases (i) and (ii) provide a good fit to the data of Theodorsen and Regier; case (iii) fits the data of Owen, who attributed the premature transition to atmospheric disturbances created by the electric motor that rotated the disc. For $\mathrm{Re}_\phi>10^6$, the three cases converge to a single curve that is in close agreement with the data and with Dorfman's relationship:[17]

$$C_m=0.982(\log_{10}\mathrm{Re}_\phi)^{-2.58} \tag{4.6}$$

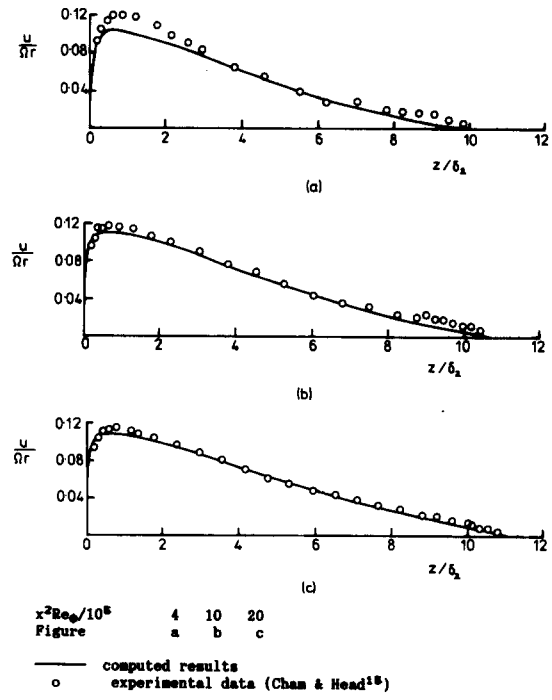

Figure 5 Axial profiles of radial component of velocity for turbulent flow over the free disc

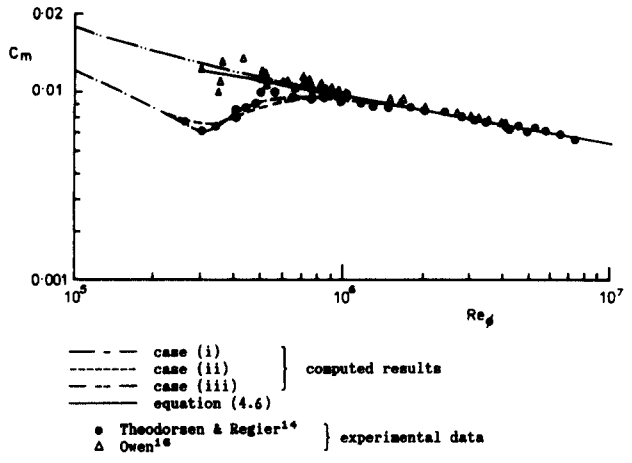

Figure 6 Moment coefficients for the free disc

5. Results for a heated disc

5.1 Definition of Nusselt numbers

Commonly used definitions of local and average Nusselt numbers are

$$\mathrm{Nu}=\frac{q_s r}{k(T_s-T_\infty)} \quad \text{and} \quad \mathrm{Nu}_{av}=\frac{q_{s,av} b}{k(T_s-T_\infty)_{av}} \tag{5.1}$$

where the subscript av refers to the radially weighted average value. However, at high Reynolds numbers where the effects of viscous dissipation can be significant, it is more appropriate to use the adiabatic-disc temperature, $T_{s,ad}$, rather than the ambient temperature, T_∞. Owen and Rogers[3] give

$$T_{s,ad}=T_\infty+\frac{\frac{1}{2}R\Omega^2 r^2}{C_p} \tag{5.2}$$

(where the recovery factor, R, is usually assumed to be equal to $\mathrm{Pr}^{1/3}$), and this leads to the alternative definitions of Nusselt numbers:

$$\mathrm{Nu}^*=\frac{q_s r}{k(T_s-T_{s,ad})} \quad \text{and} \quad \mathrm{Nu}^*_{av}=\frac{q_{s,av} b}{k(T_s-T_{s,ad})_{av}} \tag{5.3}$$

5.2 Comparison with existing theory

It is convenient to consider "power-law" disc-temperature distributions of the form

$$T_s-T_{ref}\propto r^n \tag{5.4}$$

where n may be positive or negative. Dorfman[17] obtained solutions of the integral equations, based on the Reynolds analogy, and his results can be expressed as

$$\mathrm{Nu}=0.308\mathrm{Pr}^{1/2}(n+2)^{1/2}(x^2\mathrm{Re}_\phi)^{1/2} \tag{5.5}$$

and

$$\mathrm{Nu}_{av}=0.308\mathrm{Pr}^{1/2}(n+2)^{1/2}\mathrm{Re}_\phi^{1/2} \tag{5.6}$$

for laminar flow with $n>-2$, and

$$\mathrm{Nu}=0.0197\mathrm{Pr}^{0.6}(n+2.6)^{0.2}(x^2\mathrm{Re}_\phi)^{0.8} \tag{5.7}$$

and

$$\mathrm{Nu}_{av}=0.0197\mathrm{Pr}^{0.6}(n+2)(n+2.6)^{-0.8}\mathrm{Re}_\phi^{0.8} \tag{5.8}$$

for turbulent flow with $n>-2.6$.

A number of authors have obtained similarity solutions for the laminar energy equation for various values of n and Pr. Some of their results are shown in Table 1, together with Dorfman's solution and results obtained using the numerical method described in Sections 2 and 3. For $-3\leqslant n\leqslant 3$, $0.1\leqslant \mathrm{Pr}\leqslant 10$, the present computations agree closely with the similarity solutions obtained by Rogers (see Owen and Rogers[3] and note that Rogers used $\mathrm{Pr}=0.71$ for air rather than the value of 0.72 used by the other authors). It should also be noted that Dorfman's Equation 5.5 is only accurate for $\mathrm{Pr}=1$, $n=2$ (the conditions for which the Reynolds analogy is valid).

The negative Nusselt numbers (which occur in laminar flow for $n<-2$ and which can also occur in turbulent flow for negative values of n) can be explained by considering the flow of cold fluid over a hot disc. The fluid close to the disc surface decreases in temperature, as it moves radially outward in the boundary layer at a slower rate than the disc itself. Consequently, heat is transferred *to* the disc despite the fact that fluid outside the boundary layer is *colder* than the disc! A turning point in the temperature profile produces a reverse gradient at the disc surface. (Nu can also become negative, in both laminar and turbulent flow, when viscous dissipation causes frictional heating of the disc; the use of Nu* rather than Nu can avoid the occurrence of negative Nusselt numbers under these conditions.)

5.3 Comparison with experimental data: average Nusselt numbers

Cobb and Saunders[20] measured the average Nusselt numbers for an isothermal disc ($n=0$) rotating about a horizontal axis in air ($\mathrm{Pr}=0.72$) in the Reynolds number range $10^4<\mathrm{Re}_\phi<6\times10^5$, with transition from laminar to turbulent flow occurring at $\mathrm{Re}_\phi\simeq 2.4\times10^5$. For $\mathrm{Re}_\phi<2\times10^5$, their results were correlated by

$$\mathrm{Nu}_{av}=0.36\mathrm{Re}_\phi^{1/2} \tag{5.9}$$

which is approximately 10% higher than the present laminar computations (and the results of Rogers and of Hartnett and Deland). This "error" is attributed to the effects of natural convection and radiation, both of which can be significant at the low values of Nu associated with experiments conducted under laminar-flow conditions. For turbulent flow, Cobb and Saunders extrapolated their results to produce the correlation

$$\mathrm{Nu}_{av}=0.15\mathrm{Re}_\phi^{0.8} \tag{5.10}$$

which agrees with Dorfman's Equation 5.8.

McComas and Hartnett[21] also measured the average Nusselt numbers for an isothermal disc rotating in air for $2\times10^4<\mathrm{Re}_\phi<6\times10^5$. Owen, Haynes and Bayley[22] made measurements on a disc with a nonuniform temperature (approximated by $n=2$) rotating in air for $2\times10^5<\mathrm{Re}_\phi<4\times10^6$. They correlated their results by

$$\mathrm{Nu}^*_{av}=0.0171\mathrm{Re}_\phi^{0.814} \tag{5.11}$$

which agrees with the Reynolds analogy applied to the measured moment coefficients of Owen.[16] (The absence of transitional effects was attributed to the atmospheric disturbances referred to in Section 4.2.)

Figure 7 shows a comparison between the preceding data and the computations based on the methods described in Sections 2 and 3. For both the isothermal and quadratic computations ($n=0, 2$), transition was assumed to occur at $x^2\mathrm{Re}_\phi=1.85\times10^5$. It can be seen that the computed curves provide a good fit to most of the data for $n=0$ but are lower than the data for $n=2$. Both computed curves are in reasonable agreement with Dorfman's turbulent result, Equation 5.8. (It should be noted that, although Nu^*_{av} is used in Figure 7, the difference between Nu_{av} and Nu^*_{av} is unlikely to be significant for $\mathrm{Re}_\phi<10^6$.)

Table 1 The effect of Prandtl number (Pr) and the power-law index (n) on $Nu(x^2 Re_\phi)^{-1/2}$ for laminar flow over a free disc

	Pr=0.1				Pr=0.72			
n	Present study	Owen and Rogers[3]	Hartnett and Deland[18]	Sparrow and Gregg[19]	Present study	Owen and Rogers (Pr=0.71)	Hartnett and Deland	Dorfman's approx. sol. (Equation 5.5)
−3	−0.0437	−0.0438			−0.3000	−0.2952		
−2	0	0			0	0		0
−1	0.0400	0.0399			0.1911	0.1893		0.265
0	0.0766	0.0766	0.0766	0.076581	0.3286	0.3259	0.330	0.375
1	0.1105	0.1104	0.110		0.4353	0.4319	0.437	0.459
2	0.1418	0.1417	0.141		0.5223	0.5185	0.524	0.530
3	0.1710	0.1709			0.5960	0.5918		

	Pr=1.0					Pr=10.0			
n	Present study	Owen and Rogers	Hartnett and Deland	Sparrow and Gregg	Dorfman's approx. sol. (Equation 5.5)	Present study	Owen and Rogers	Hartnett and Deland	Sparrow and Gregg
−3	−0.4071	−0.4074				−3.1092	−3.057		
−2	0.0002	0			0	0.0004	0		
−1	0.2351	0.2352			0.308	0.7357	0.7368		
0	0.3962	0.3962	0.396	0.39625	0.436	1.1335	1.134	1.13	1.1341
1	0.5180	0.5180	0.518		0.533	1.4079	1.408	1.41	
2	0.6159	0.6159	0.616		0.616	1.6201	1.621	1.62	
3	0.6982	0.6982				1.7953	1.796		

	Pr=100.0		
n	Present study	Hartnett and Deland	Sparrow and Gregg
−3	−19.329		
−2	0.0012		
−1	1.7982		
0	2.6857	2.69	2.6871
1	3.2830	3.28	
2	3.7143	3.71	
3	4.1181		

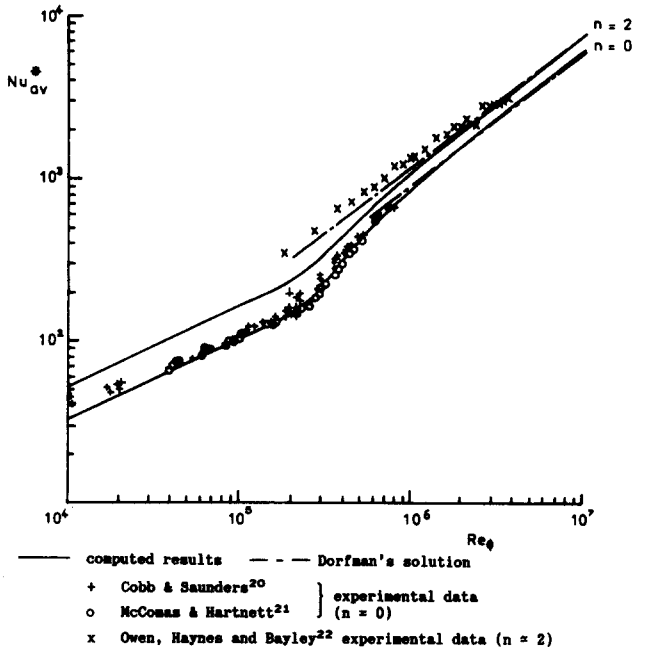

Figure 7 Average Nusselt numbers for the free disc rotating in air

5.4 Comparison with experimental data: local Nusselt numbers

Northrop and Owen[23] obtained local Nusselt numbers for a disc rotating in air at Reynolds numbers up to $Re_\phi = 3.2 \times 10^6$. The disc-temperature distribution could be varied by means of built-in electric heaters, and the Nusselt numbers could be obtained both from fluxmeters and from solution of the conduction equations for the disc itself. The four disc-temperature distributions tested were approximated by power laws with $n \simeq -0.2$, 0.1, 0.4, and 0.6. The local Nusselt numbers, measured by fluxmeters, are shown in Figures 8–11. Computations of the Nusselt numbers were obtained using disc temperatures as boundary conditions for the energy equation. As the original raw data were unavailable, the disc temperatures were obtained from the smoothed data found in Northrop's thesis;[24] further details are given by Ong.[13]

Figure 8, for $n \simeq -0.2$, shows that, apart from the lower values of Re_ϕ, the agreement between the computed and measured Nusselt numbers is good. The underestimate of the measured values at the lower Re_ϕ is believed to be caused by the effects of radiation and natural convection, which were also

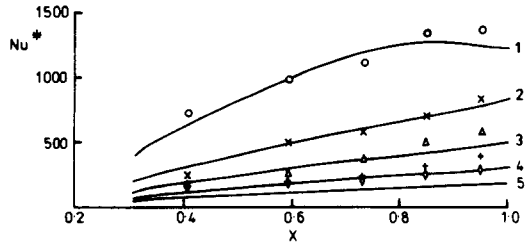

Re_ϕ	Experimental data (Northrop & Owen[23])	Computed results
2.65×10^6	o	1
1.08×10^6	x	2
5.48×10^5	Δ	3
2.72×10^5	+	4
1.40×10^5	◊	5

Figure 8 Radial variation of local Nusselt numbers for the free disc (Pr=0.71, $n\approx-0.2$)

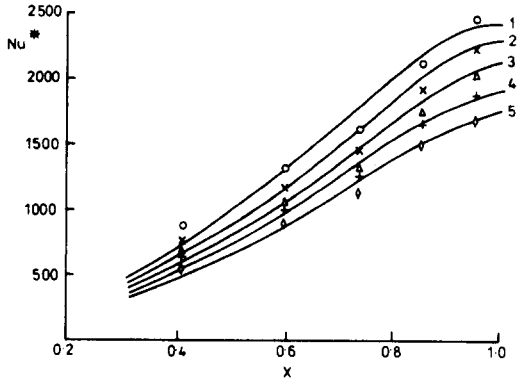

Re_ϕ	Experimental data (Northrop & Owen[23])	Computed results
3.20×10^6	o	1
2.66×10^6	x	2
2.40×10^6	Δ	3
2.14×10^6	+	4
1.88×10^6	◊	5

Figure 9 Radial variation of local Nusselt numbers for the free disc (Pr=0.71, $n\approx0.1$)

mentioned in Section 5.3. The fall-off in Nu* for large values of x at $Re_\phi=2.65\times10^6$ is attributed to the local disc-temperature distribution.

Similar trends can be seen in Figures 9–11, which serve to illustrate that, for a given Reynolds number, Nu* increases as n increases and, for a given value of n, Nu* increases as Re_ϕ increases. Overall, there is good agreement between the computed and measured Nusselt numbers, which gives confidence in the accuracy of both.

6. Conclusions

The boundary-layer momentum and energy equations for the free disc have been solved using a Keller-box finite-difference scheme and the Cebeci and Smith[8] eddy-viscosity model.

For isothermal laminar flow, the computed velocity distributions and moment coefficients are in good agreement with both analytical solutions and experimental data. For isothermal turbulent flow, the computations agree well with the available experimental data.

For the case of a heated disc, the computations of the Nusselt numbers for laminar flow agree closely with the solutions of other authors for a wide range of Prandtl numbers and disc-temperature distributions. For both laminar and turbulent flow, the computed average and local Nusselt numbers are in good agreement with the available experimental data. Although the experiments were all performed in air, the data were obtained over a wide range of disc-temperature distributions and for Reynolds numbers up to $Re_\phi=3.2\times10^6$.

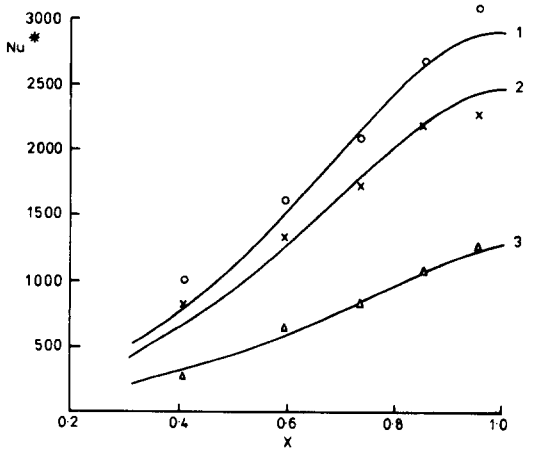

Re_ϕ	Experimental data (Northrop & Owen[23])	Computed results
3.14×10^6	o	1
2.67×10^6	x	2
1.08×10^6	Δ	3

Figure 10 Radial variation of local Nusselt numbers for the free disc (Pr=0.71, $n\approx0.4$)

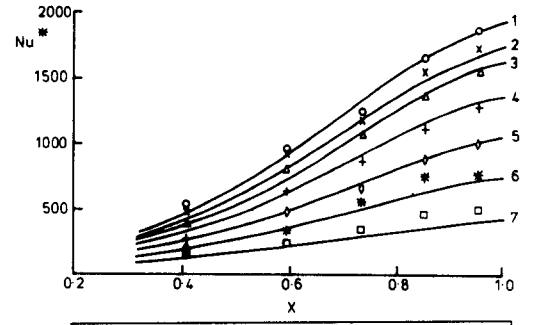

Re_ϕ	Experimental data (Northrop & Owen[23])	Computed results
1.71×10^6	o	1
1.59×10^6	x	2
1.36×10^6	Δ	3
1.11×10^6	+	4
8.25×10^5	◊	5
5.52×10^5	*	6
2.80×10^5	□	7

Figure 11 Radial variation of local Nusselt numbers for the free disc (Pr=0.71, $n\approx0.6$)

The method of solution used here is shown to be sufficiently simple, efficient, and accurate for all practical purposes. It can be readily extended to other rotating-disc problems, as demonstrated by Ong and Owen.[25,26]

Acknowledgments

We wish to thank the Science and Engineering Research Council, Rolls Royce plc, and Ruston Gas Turbines plc for supporting the work described in this article. The research was conducted while we were at the Thermo-Fluid Mechanics Research Centre at the University of Sussex.

References

1 Kármán, Th. von. Über laminare und turbulente Reibung. *Z. angew. Math. Mech.*, 1921, **1**, 233
2 Cochran, W. G. The flow due to a rotating disk. *Proc. Camb. Phil. Soc.*, 1934, **30**, 365
3 Owen, J. M. and Rogers, R. H. *Flow and heat transfer in rotating-disc systems. Vol. 1 Rotor-stator systems.* Research Studies Press, Taunton, UK, 1989
4 Cooper, P. Turbulent boundary layer on a rotating disk calculated with an effective viscosity. *AIAA J.*, 1971, **9**, 255
5 Koosinlin, M. L. Turbulent transport properties in swirling two-dimensional boundary layers. Ph.D. thesis, Imperial College of Science and Technology, 1974
6 Launder, B. E. and Sharma, B. I. Application of the energy-dissipation model of turbulence to the calculation of flow near a spinning disc. *Letters in Heat and Mass Transfer*, 1974, **1**, 131
7 Cebeci, T. and Abbott, D. E. Boundary layers on a rotating disc. *AIAA J.*, 1975, **13**, 829
8 Cebeci, T. and Smith, A. M. O. *Analysis of Turbulent Boundary Layers.* Academic Press, New York, 1974
9 Jones, W. P. and Launder, B. E. The calculation of low-Reynolds-number phenomena with a two-equation model of turbulence. *Int. J. Heat Mass Transfer*, 1973, **16**, 1119
10 Cebeci, T. Kinematic eddy viscosity at low Reynolds numbers. *AIAA J.*, 1973, **11**, 102
11 Gregory, N., Stuart, J. T., and Walker, W. S. On the stability of three-dimensional boundary layers with application to the flow due to a rotating disk. *Phil. Trans. Roy. Soc.*, 1955, **A248**, 155
12 Keller, H. B. A new difference scheme for parabolic problems. *Proc. 2nd Symp. on Num. Sol. of Partial Diff. Eqs.* Academic Press, New York, 1971
13 Ong, C. L. Computation of fluid flow and heat transfer in rotating-disc systems. D.Phil. thesis, University of Sussex, 1988
14 Theodorsen, T. and Regier, A. Experiments on drag of revolving disks, cylinders, and streamline rods at high speeds. *NACA Rep.* No. 793, 1944
15 Cham, T. S. and Head, M. R. Turbulent boundary-layer flow on a rotating disk. *J. Fluid Mech.*, 1969, **37**, 129
16 Owen, J. M. Flow between a rotating and a stationary disc. D.Phil. thesis, University of Sussex, 1969
17 Dorfman, L. A. *Hydrodynamic Resistance and the Heat Loss of Rotating Solids.* Oliver and Boyd, Edinburgh, 1963
18 Hartnett, J. P. and Deland, E. C. The influence of Prandtl number on the heat transfer from rotating nonisothermal disks and cones. *J. Heat Transfer*, 1961, **83**, 95
19 Sparrow, E. M. and Gregg, J. L. Heat transfer from a rotating disk to fluids of any Prandtl number. *J. Heat Transfer*, 1959, **81**, 249
20 Cobb, E. C. and Saunders, O. A. Heat transfer from a rotating disk. *Proc. R. Soc.*, 1956, **A236**, 343
21 McComas, S. T. and Hartnett, J. P. Temperature profiles and heat transfer associated with a single disk rotating in still air. *Proc. 4th Int. Heat Transfer Conf.*, Paris-Versailles, III. FC7.7, 1970
22 Owen, J. M., Haynes, C. M., and Bayley, F. J. Heat transfer from an air-cooled rotating disk. *Proc. R. Soc.*, 1974, **A336**, 453
23 Northrop, A. and Owen, J. M. Heat transfer measurements in rotating-disc systems. Part I: The free disc. *Int. J. Heat and Fluid Flow*, 1988, **9**, 19
24 Northrop, A. Heat transfer in a cylindrical cavity. D.Phil. thesis, University of Sussex, 1984
25 Ong, C. L. and Owen, J. M. Boundary-layer flows in rotating cavities. *J. Turbomachinery*, 1989, **111**, 341
26 Ong, C. L. and Owen, J. M. Prediction of heat transfer in a rotating cavity with a radial outflow. 34th ASME Int. Gas Turbine Conf., Toronto, 1989, Paper No. 89-GT-286